Zero-field splitting of the $4f^7$ state: A systematic investigation of Gd^{3+}-M^+ complexes in CaF_2

E. J. Bijvank and H. W. den Hartog
Solid State Physics Laboratory, 1 Melkweg, 9718 EP Groningen, The Netherlands
(Received 17 April 1980)

In this paper we present an analysis of the results of various experiments [electron paramagnetic resonance (EPR), electric field effect (EFE) in EPR, and electron-nuclear double resonance (ENDOR)] on orthorhomic Gd^{3+}-M^+ complexes in CaF_2. From the detailed and systematic study of the series of complexes (M^+ = Li, Na, K, Rb, and Cs), we obtain a consistent picture of the mechanisms giving rise to the zero-field splitting of Gd^{3+} in ionic materials, a problem that has puzzled scientists for a number of years. It appears that the zero-field splittings for the systems investigated can be explained in terms of a self-consistent polarizable-point-charge model using coupling mechanisms published in the literature. This conclusion is in contrast with those drawn by several authors in the literature and leads to a reconsideration of the merits of the polarizable-point-charge model.

I. INTRODUCTION

We have investigated in earlier papers[1–4] the effect of the size of the compensating monovalent metal ion (M^+) on the crystal-field parameters of trivalent Gd^{3+} in local charge compensation centers in cubic alkaline-earth halides; a schematic representation of these centers is given in Fig. 1. These defects can be studied easily because our crystal growth techniques allow us to introduce sufficient concentrations in the materials used for our experiments: CaF_2, SrF_2, BaF_2, and $SrCl_2$. In the crystals mentioned most of the orthorhombic (C_{2v}) Gd^{3+}-M^+ centers (where M^+ refers to a monovalent alkali ion) can be studied by means of the EPR technique. For the electric field effect (EFE) and the electron-nuclear double resonance (ENDOR) experiments, crystals with high defect concentrations are required; in addition, the EPR lines should be as narrow as possible. These conditions limit the number of combinations that can be investigated by means of this technique.

It is the purpose of this paper to combine the results of EPR, EFE, and ENDOR experiments in order to obtain a consistent picture of (i) the mechanisms that give rise to the second-degree crystal-field splitting for Gd^{3+} in ionic crystals; (ii) the displacements of the ions surrounding the Gd^{3+}-M^+ complex. Useful information concerning these properties has been obtained from a systematic series of experiments in which the different experimental techniques provide us with parameters determined independently. Especially the effects of the ionic radii of the M^+ impurities, which vary from 0.68 Å for Li^+ to 1.67 Å for Cs^+, have contributed significantly to the level of understanding.

Lefferts, Bijvank, and den Hartog[3] have shown that odd crystal-field terms contribute to the zero-field splitting of Gd^{3+}; therefore, we have taken this effect into account in the present treatment. In some cases this contribution may lead to a change of sign of the parameter B_2^0. From theory we have found that the odd crystal-field contributions to B_2^2 are negligible; this has been confirmed by our experimental results.

It is obvious that with increasing M^+ radius the ions neighboring the M^+ impurity will relax away from the lattice positions. The zero-field splitting of the Gd^{3+} ion depends strongly upon the contributions from the fluoride ions neighboring this impurity; thus for a description of the zero-field-splitting parameters the positions of the fluoride ions neighboring both Gd^{3+} and M^+ are important parameters to determine. Unfortunately, ENDOR is not a conclusive technique for the determination of positions of the first coordi-

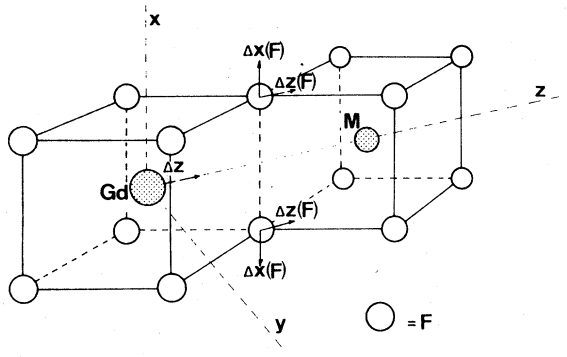

FIG. 1. Three-dimensional schematic representation of a Gd^{3+}-M^+ complex in CaF_2. The system of axes has been indicated by x, y, and z; $\Delta x(F)$, $\Delta z(F)$, and $\Delta z(Gd)$ represent parameters used in Sec. III B.

nation shell. ENDOR gives important information about the positions of more distant fluoride ions. From a comparison of the EPR and the EFE results we have been able to find a set of displacement parameters of the first-shell fluoride ions mentioned above. These displacement parameters are consistent with the results of both techniques. It should be emphasized that all calculations are based upon the polarizable-point-charge model, which appears to work satisfactorily for the ionic materials under investigation.

II. EXPERIMENTAL PROCEDURES

The methods employed for the preparation of the crystals have been described in Refs. 2 and 3. Special attention has been paid to optimize the growth conditions to obtain materials with narrow EPR and ENDOR lines.

The EPR and ENDOR experiments have been carried out with a Varian E-line Century Series setup. The magnetic field strength is Hall controlled. The NMR power (up to 10 W) is applied to a coil mounted onto the quartz tail of an insertion cryostat containing liquid He. The crystal, which is surrounded by the liquid He, is rotatable about a vertical axis, usually chosen parallel to [110]. Also, rotation of the cryostat is independent of that of the crystal. This allows us to find the maximum ENDOR signal intensity without losing the orientation of the crystal with respect to the magnetic field direction.

In the ENDOR experiments the magnetic field strength is kept at a constant value, such that the observed signal intensity shows a maximum; this signal is detected using 100-kHz magnetic field modulation. The NMR field is obtained by a Hewlett-Packard HP 8601A sweep generator capable of generating frequencies up to 110 MHz. This frequency is modulated by an external source (400 Hz). The 400-Hz component of the signal is amplified by means of a lock-in amplifier. In order to obtain maximum NMR power in the coil, the circuit containing the coil was kept in resonance by means of a variable capacitor. For our setup this could be done for the frequency range 2–30 MHz. This range can be extended easily by exchanging the coil system.

Using good quality crystals (0.15 cm^3) we obtained ENDOR spectra of cubic Gd^{3+} with a signal-to-noise ratio of 100 for an RC time of 0.3 sec. The ENDOR spectra of the Gd^{3+}-K^+ complexes are much more difficult to detect because the concentration of these defects is lower than that of cubic Gd^{3+}; in addition, the EPR and ENDOR lines are generally split, leading to an appreciable reduction of the signal intensity. For the best crystals a typical value of the signal-to-noise ratio is 30 at an RC time of 3 sec.

III. EXPERIMENTAL RESULTS

A. EFE experiments

In order to obtain more information about the origin of the crystal-field splitting of trivalent gadolinium ions it was found necessary to investigate the strength of the parameters associated with the odd crystal-field interaction.[3,5,6] In an earlier paper[3] we found values for the odd crystal-field parameter c_1^0 for complexes of the type Gd^{3+}-Li^+, Gd^{3+}-K^+, and Gd^{3+}-Ag^+ in CaF_2. The result of an EFE experiment on Gd^{3+}-Na^+ complexes in CaF_2 has been given in Fig. 2. The experiment has been carried out on the EPR transition $-\frac{5}{2} \leftrightarrow -\frac{7}{2}$; the magnetic field direction is along the $[1\bar{1}0]$ axis and the Gd^{3+}-Na^+ complex is oriented along the [110] axis. The electric field is also along [110]. Figure 2 shows that the electric field broadens the EPR line due to the fact

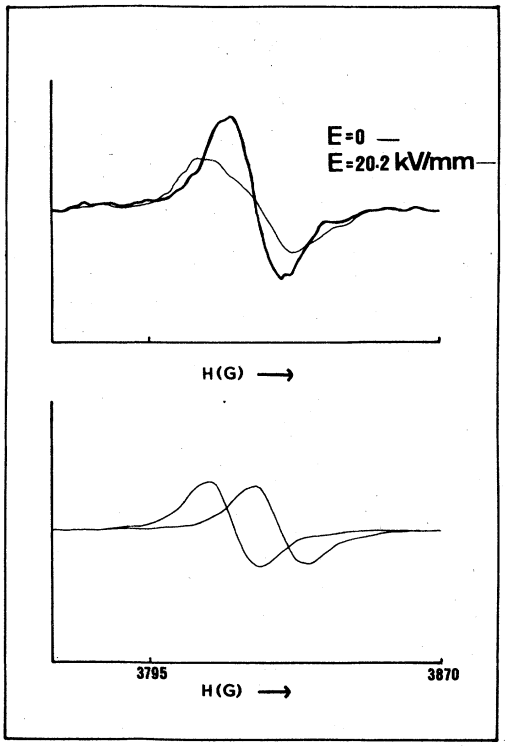

FIG. 2. EFE of the $-\frac{5}{2} \leftrightarrow -\frac{7}{2}$ transition of a Gd^{3+}-Na^+ complex. The z axis of the complex is along [110] as is the electric field $\vec{E}$. The magnetic field is chosen along $[1\bar{1}0]$. In the upper curve we show the changes of the EPR line when an electric field of 20.2 kV/mm is applied. The broadened line in the upper figure is a superposition of two EPR lines which have shifted into opposite directions (see lower figure). The two traces shown in the lower figure have been calculated theoretically from a fitting procedure; they should add up to the broadened line in the upper figure.

that the line splits up into two components. One of the lines is associated with complexes parallel to the electric field and the other line is due to complexes which are antiparallel to the electric field. The two lines are not resolved but the splitting can be obtained by fitting the displacement of the lines by means of a computer. The result has been shown in the lower part of Fig. 2.

In Fig. 3 we show the splitting of the EPR lines as a function of the applied electric field. Reliable results are obtained for electric field strengths larger than about 10 kV/mm. From Fig. 3 it is clear that we are dealing with a linear electric field effect, consistent with the lack of inversion symmetry; the system under consideration[1-4] has orthorhombic symmetry (C_{2v}). Unfortunately, we can only study the EFE of "perpendicular" complexes because the $-\frac{5}{2} \leftrightarrow -\frac{7}{2}$ transition associated with "parallel" complexes is hidden under the cubic transitions which are far stronger in intensity. This is in contrast with the results obtained for Gd^{3+}-K^+ and Gd^{3+}-Ag^+, where the lines associated with the $-\frac{5}{2} \leftrightarrow -\frac{7}{2}$ transition of parallel complexes are quite well observable for $\vec{H} \parallel [110]$. The advantage of studying the EFE of EPR lines due to parallel complexes is that the induced splitting is a factor of 2 larger than for perpendicular complexes. The EFE of parallel complexes has been studied for Gd^{3+}-Rb^+ in CaF_2. Here too, we have chosen the $-\frac{5}{2} \leftrightarrow -\frac{7}{2}$ transition as it gives the largest splitting between the individual lines connected with parallel and antiparallel complexes. It can be seen from Fig. 4 that the results are reliable for field strengths higher than about 22 kV/mm. This limitation on the reliability is due to the larger linewidth of the signal used for the EFE experiment; also the magnitude of the EFE is smaller. In addition the intensity of the signal was smaller, which is caused by the fact that Rb^+ ions are difficult to introduce into the CaF_2 crystal. The transition investigated is located at 6090 G and the conditions are $\vec{H} \parallel [110]$ and $\vec{E} \parallel [110]$.

Until now we have only investigated the electric field effect of charge compensation centers with their symmetry axis along $\vec{E}$ and the magnetic field $\vec{H}$ parallel or perpendicular to $\vec{z}$. It can be shown that these types of experiments only give limited information about the odd terms in the spin Hamiltonian. In order to learn more about these parameters, electric field effect experiments have been carried out for different angles between the electric field direction and the magnetic field direction. For these experiments we have used calcium fluoride crystals doped with Gd^{3+} and Na^+ because for Gd^{3+}-Na^+ complexes we have observed relatively large electric field effects. If the electric field is along the z axis of the complex and the angle between the $\vec{z}$ and $\vec{H}$ is θ, the splitting

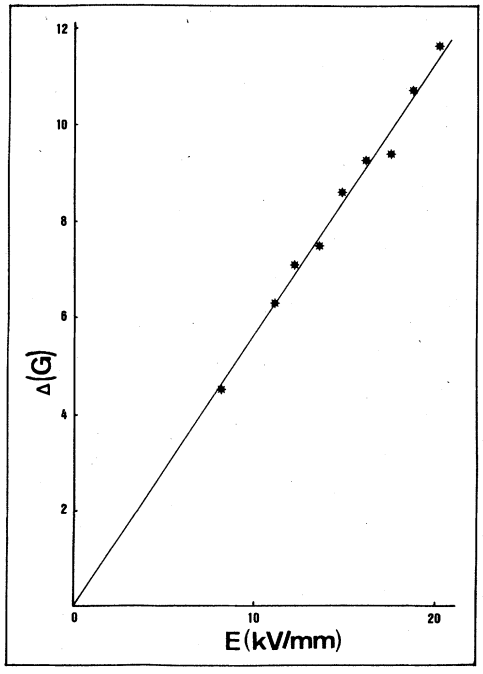

FIG. 3. Linear EFE of the $-\frac{5}{2} \leftrightarrow -\frac{7}{2}$ transition of perpendicular Gd^{3+}-Na^+ complexes in CaF_2, i.e., $\vec{z} \parallel [110]$ and $\vec{H} \parallel [1\bar{1}0]$. In this experiment $\vec{E} \parallel [110]$.

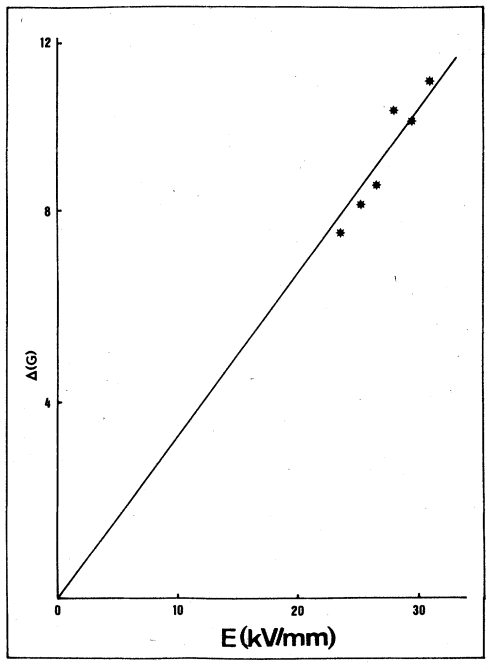

FIG. 4. Linear EFE of the $-\frac{5}{2} \leftrightarrow -\frac{7}{2}$ transition of parallel Gd^{3+}-Rb^+ complexes in CaF_2; here, $\vec{H} \parallel [110]$, $\vec{E} \parallel [110]$, and $\vec{z} \parallel [110]$.

TABLE I. Crystal-field parameter B_2^0 of Gd^{3+}-M^+ complexes in CaF_2 as measured with EPR (Ref. 2). B_2^{0*} is the contribution to B_2^0 from the even electrostatic crystal-field term only.

M^+	B_2^0 (G)	B_2^{0*} (G)
Li^+	17.7	−21.7
Na^+	3.4	−31.9
K^+	83.6	71.3
Rb^+	141.8	138.7
Ag^+	50.9	22.2

of the $-\frac{3}{2} \leftrightarrow -\frac{5}{2}$ transition can be written as

$$\Delta = 12[(3\cos^2\theta - 1)B_2^0(\mathrm{EFE}) + \sin^2\theta B_2^2(\mathrm{EFE})] \ , \tag{1}$$

and $\vec{H}$ in the yz plane of the complex under consideration. We have investigated closely the situation where $\theta = 54.7°$; here $(3\cos^2\theta - 1) = 0$ and we only deal with the contribution associated with $B_2^2(\mathrm{EFE})$. For electric field strengths up to 30 kV/mm, no evidence for an electric effect has been observed and because in this situation

$$\Delta = 8B_2^2(\mathrm{EFE}) \ , \tag{2}$$

we conclude that $B_2^2(\mathrm{EFE})$ is very small or zero. We note that this has been predicted by Bijvank, den Hartog, and Andriessen[2] from a theoretical treatment on the basis of the equivalent even field method proposed by Kiel and Mims[7,8] and Parrot.[6] From this result it is concluded that the second-order contributions to the crystal-field parameter B_2^2 as proposed by Bijvank, den Hartog, and Andriessen,[2] caused by odd crystal-field terms are small or zero for orthorhombic symmetry. This is in contrast with the results for B_2^0; it can be shown that second-order contributions due to first-degree crystal-field terms can be quite significant. In some cases these contributions change the sign of the parameter B_2^0 (see Table I) and therefore a careful study of the first-degree crystal-field parameters is of importance for the understanding of the phenomenon of the zero-field splitting of Gd^{3+} in crystalline hosts.

B. Combined interpretation of EFE and crystal-field measurements

The linear electric field effect has been employed by Lefferts *et al.*[3] to check the polarizable-point-charge model, which has been widely used to calculate the zero-field splitting of Gd^{3+} impurities in crystalline hosts. These authors have shown that this model accounts roughly for the trends observed for both the EFE experiments and the crystal-field splitting.

In the present investigation we have considered the new EFE results and found that relaxation of the Gd^{3+} impurity with respect to its immediate surroundings is quite important to obtain a consistent picture of both the EFE and crystal-field splitting results. It turns out that with three displacement parameters: $\Delta z(\mathrm{Gd})$, $\Delta z(\mathrm{F})$, and $\Delta x(\mathrm{F})$ (see Fig. 1) the experimental results for the crystal-field splitting and the EFE can be explained reasonably well. The magnitudes of the various displacement parameters are in agreement with the expectations based on considerations of the relative sizes of the monovalent impurities and the excess negative charge within the point-charge model.

Another advantage of the method employed here is that the dipoles induced at the various ions in the neighborhood of the defect are calculated using the total electric field at the ions including contributions from effective dipoles due to ions shifted from the cubic lattice sites and dipoles induced by the presence of electric fields. This interdependence implies that we had to employ an iterative approach such that first the electric fields are calculated, then the induced dipoles are evaluated and in the next step the electric fields at the ions are calculated using the new induced dipole moments. This procedure is repeated several times until the electric fields at the ions are stabilized; subsequently, the theoretical EFE and the crystal-field splitting parameters can be calculated. A detailed survey of the method has been presented in Appendix A. The contributions that point charges give to the various crystal-field splitting parameters have been given in Refs. 2 and 3. Contributions due to "displacement dipoles" and induced dipoles can easily be calculated (see Appendix A).

It was shown in our earlier papers that we are able to describe the observed crystal-field parameters quite satisfactorily by means of Eqs. (8) and (9) of Ref. 2. However, we note that we have seen[3] that the results of electric field effect experiments on Gd^{3+}-M^+ complexes in CaF_2 deviate from the expected values by approximately a factor of 3, indicating that either the odd field contribution to the crystal-field parameter B_2^0 or the description of the coupling between the even crystal field and the magnetic energy levels is insufficient.

In order to check the uncertainties in the models we have varied the proportionality factors occurring in the relations describing B_2^0, B_2^2, and c_1^0. According to Refs. 2 and 3 we can write

$$B_2^0 = 10.20 \times 10^{-18} c_2^0 + 4.980 \times 10^{-19} (c_1^0)^2 \ , \tag{3}$$

and

$$B_2^2 = 10.20 \times 10^{-18} c_2^2 \ . \tag{4}$$

TABLE II. Experimental and calculated crystal-field parameters B_2^0, B_2^2, and c_1^0 for the different alkali ions in a Gd^{3+}-M^+ complex in CaF_2. The theoretical values have been fitted to the experimental ones on the basis of Eqs. (5) and (6); the associated displacement parameters have been given in Table III.

M^+	B_2^0 (G) Expt.	Theor.	B_2^2 (G) Expt.	Theor.	$\lvert c_1^0 \rvert$ (10^9 V/m) Expt.	Theor.
Li^+	17.7	18.3	−46.6	−51.1	7.5	(−) 6.5
Na^+	3.4	3.1	−30.0	−28.5	7.1	(−) 6.7
Ag^+	50.9	55.2	−26.3	−25.8	6.4	(−) 3.2
K^+	83.6	78.3	−20.1	−30.0	4.2	(−) 2.3
Rb^+	141.8	146.5	−11.9	−10.4	2.1	1.9
Cs^+	220.5	110.2	−4.0	2.8	· · ·	4.1

The factor 10.20×10^{-18} comes from Hutchison, Judd, and Pope[9] coupling mechanism and the Wybourne mechanism.[10] The contribution to B_2^0 due to odd crystal-field interactions has been calculated using the Kiel[7] and the Parrot[6] mechanism. It has been found that the proportionality factors occurring in Eqs. (3) and (4) are not fully certain since we know too little about the mechanisms giving rise to the crystal-field splitting and the EFE. Especially the relations describing the EFE given in Ref. 3 [Eqs. (10) and (11)] contain various contributions of opposite signs and approximately the same magnitude. We have found that an increased value of this factor leads to an improved overall explanation of our experimental observations. The relations

$$B_2^0 = 10.20\times10^{-18}c_2^0 + 7\times10^{-19}(c_1^0)^2 \ , \qquad (5)$$

and

$$B_2^2 = 10.20\times10^{-18}c_2^2 \ , \qquad (6)$$

give the best description of the experimental observations if only the proportionality factor associated with the contribution to the odd crystal-field terms is varied; values smaller than 4.98×10^{-19} need very large displacements of the Gd impurity. Also the results in accordance with Eqs. (3) and (4) lead to a discrepancy especially for the parameter c_1^0 (compare the results in Ref. 2). If we change the proportionality factor connected with the even field contributions we also have to change the one associated with the odd fields by the same relative amount. Employing smaller proportionality factors than 10.20×10^{-18} for c_2^0 and c_2^2 leads to unrealistic results for the displacements of the Gd^{3+} impurity within the defect. The relations

$$B_2^0 = 15\times10^{-18}c_2^0 + 7.5\times10^{-19}(c_1^0)^2 \ , \qquad (7)$$

and

$$B_2^2 = 15\times10^{-18}c_2^2 \ , \qquad (8)$$

lead to a good agreement if rather large values for Δz(Gd) are chosen. More reasonable displacements of the Gd impurity are found if we employ Eqs. (5) and (6). The best fit of the parameters B_2^0, B_2^2, and c_1^0 with Eqs. (5) and (6) has been given in Table II and the associated displacement parameters have been compiled in Table III. The overall agreement between the experimental and fitted crystal-field parameters is quite satisfactory and it can be seen from Table III that the x displacement of the fluoride ions neighboring both the Gd^{3+} and the M^+ impurity shows a definite trend to increase with increasing M^+ radius. This result is similar to that obtained by Bijvank, den Hartog, and Andriessen.[2] However, the trend observed for the z displacement parameter of these fluoride ions is opposite to that observed in Ref. 2. We emphasize here that the trend shown in Table III is less definite than the one found in our earlier work. New is the displacement found for the

TABLE III. Displacement parameters Δz(Gd), Δx(F), and Δz(F) as indicated in Fig. 1 which have been fitted to the experimental crystal-field parameters using Eqs. (5) and (6).

M^+	Δz(Gd) (Å)	Δx(F) (Å)	Δz(F) (Å)
Li^+	0.10	0.05	0.04
Na^+	0.10	0.03	0.06
Ag^+	0.05	0.10	0.03
K^+	0.05	0.13	0.03
Rb^+	0.00	0.22	0.01
Cs^+	0.00	0.30	0.00

TABLE IV. Displacement parameters $\Delta z(\mathrm{Gd})$, $\Delta x(\mathrm{F})$, and $\Delta z(\mathrm{F})$ as indicated in Fig. 1 which have been fitted to the experimental crystal-field parameters on the basis of Eqs. (7) and (8).

M^+	$\Delta z(\mathrm{Gd})$ (Å)	$\Delta x(\mathrm{F})$ (Å)	$\Delta z(\mathrm{F})$ (Å)
Li^+	0.15	0.047	0.08
Na^+	0.15	0.035	0.09
Ag^+	0.15	0.075	0.08
K^+	0.10	0.098	0.055
Rb^+	−0.05	0.14	0.035
Cs^+	−0.05	0.24	0.028

Gd^{3+} ion which turns out to be significant for small M^+ ions and decreases for increasing M^+ radii. For the Gd^{3+}-K^+ complex we have found a value of $\Delta z(\mathrm{Gd}) = 0.05$ Å, which agrees reasonably well with the results of ligand ENDOR experiments on these complexes in CaF_2, reported in Sec. III C of this paper.

The displacements obtained with the alternative formulas (7) and (8) have been compiled in Table IV. The corresponding fit of the parameters is of about the same quality as the fit shown in Table II. It is obvious from Table IV that the displacement parameter $\Delta x(\mathrm{F})$ also increases with increasing M^+ radii, especially for $R_{M^+} > 1.0$ Å. The $\Delta z(\mathrm{F})$ values in Table IV show the same behavior as in Table III. An appreciable difference between Tables III and IV is that the shift of the Gd^{3+} ion in Table IV is significantly larger than in Table III. Also the variations as a function of the M^+ radius are larger in Table III, and there appears to be a discontinuous change of the Gd position if we replace K^+ by Rb^+. This discontinuity has not been found in the results of the calculations, which are presented in the following paper. In addition, we note that $\Delta z(\mathrm{Gd}) = 0.10$ for the Gd^{3+}-K^+ complex in CaF_2, which is too large compared with the experimental value obtained from ENDOR experiments.

C. ENDOR experiments on CaF_2:Gd^{3+}, K^+ and CaF_2:Gd^{3+}, Li^+

In order to obtain detailed information about the relaxation of the ions neighboring the complex ligand ENDOR on Gd^{3+}-K^+ and Gd^{3+}-Li^+ complexes in CaF_2 have been carried out. Special attention has been paid to the preparation of the samples to obtain as narrow absorption lines as possible. The ligand ENDOR experiments have been carried out on samples containing Gd isotopes in the natural abundances.

The ENDOR experiments have been performed with the magnetic field direction in the (110) plane and it was found that the most important information could be drawn from the experiments with $\vec{H}_0 \| \langle 110 \rangle$, $\vec{H}_0 \| \langle 100 \rangle$, and $\vec{H}_0 \| \langle 111 \rangle$, and for $\vec{H}_0$ along a direction 6° of arc away from $\langle 111 \rangle$ into the direction $\langle 110 \rangle$. For the interpretation of the ENDOR results of the orthorhombic complexes it is necessary to compare the spectra with those obtained for cubic Gd^{3+} for exactly the same orientation. This is possible because in our samples orthorhombic centers as well as cubic Gd^{3+} ions are present in sufficient concentrations. With the ligand ENDOR experiments reported here we have investigated the equilibrium positions of some F^- ions neighboring the Gd^{3+} impurity.

The positions of the ENDOR lines can be described by a spin Hamiltonian containing many terms of various different interactions even if we limit ourselves to complexes containing a Gd nucleus without a nuclear spin

$$\mathcal{H} = g\mu_B \vec{H}\cdot\vec{S} + B_2^0 O_2^0 + B_2^2 O_2^2 + B_4^0 O_4^0 + B_4^2 O_4^2 + B_4^4 O_4^4 + B_6^0 O_6^0 + B_6^2 O_6^2 + B_6^4 O_6^4 + B_6^6 O_6^6 + \sum_{j=1}^{8} (\vec{S}\vec{A}_j\vec{I}_j + g_F\mu_N \vec{H}\cdot\vec{I}_j) \quad . \tag{9}$$

It is possible to derive the values of the parameters in the spin Hamiltonian from the measured ENDOR line positions only if the complete Hamiltonian is diagonalized. This can be done by using an extended computer program as given in Ref. 2. Most important for the determination of the positions of the F^- ions neighboring the Gd^{3+} impurity are the values of the isotropic and anisotropic hyperfine interaction constants. Only more distant F^- ions can be treated by means of ENDOR results in an accurate way. If one is dealing with F^- ions neighboring the Gd^{3+} impurity, the experimental results do not allow conclusions about the positions of these ions because there are contributions to the hfs constants due to: contact interaction, classical dipole-dipole interaction, covalency, overlap, and polarization of the electron clouds.

In order to describe the charge compensation defect, we have given a three-dimensional schematic representation of the immediate surroundings in Fig. 5. This figure shows ions surrounding the Gd^{3+} impurity up to the third shell of fluoride ions. The characters associated with the fluoride ions are important because we have to distinguish between these ions when we describe the various ENDOR lines. Another complication that occurs when the ENDOR spectra are studied is that there are different orientations of the complexes in the crystal lattice. The dipoles are aligned along any of the $\langle 110 \rangle$ axes. For-

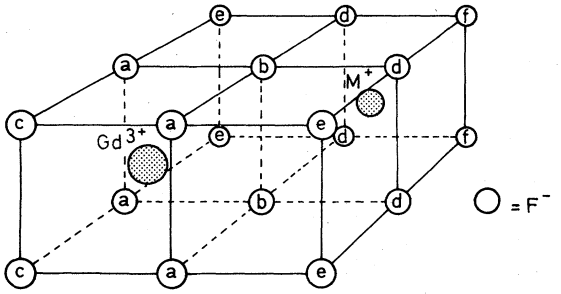

FIG. 5. Schematic representation of a Gd^{3+}-M^+ complex in CaF_2. Equivalent fluoride ions are indicated by the same character.

tunately, the EPR results are highly accurate, implying that we always knew what type of orthorhombic centers we were looking at.

We shall first consider the first coordination shell of fluoride ions. There are eight F^- ions, which can be divided into three groups: first we have two ions neighboring the Gd^{3+} and the M^+ impurity, secondly there are four ions located in the plane perpendicular to the z axis of the center, which contains the Gd^{3+} impurity and, thirdly, there are two more F^- neighbors, which are far away from the M^+ ion. It is obvious that these three different types of F^- neighbors have different displacements because of the presence of the M^+ impurity. In addition, we also expect that the Gd^{3+} impurity will be displaced from the substitutional site. For the second group of F^- ions we have found ten experimental ENDOR frequencies, which could be fitted with the spin Hamiltonian. Similarly we have obtained nine ENDOR frequencies for the F^- ions of the first and third group each. This information is not sufficient to estimate the positions of the fluoride ions under consideration as will be clarified in the following.

The extra contributions to the spin Hamiltonian due to the presence of one fluorine nucleus can be written as

$$\mathcal{H}_F = g_F \mu_N \vec{H} \cdot \vec{I} + \sum_{j,k} A_{jk} S_j I_k \ . \tag{10}$$

If the hyperfine tensor elements A_{jk} are determined by contact interactions and dipole-dipole interactions only, these tensor elements are given by the following formulas

$$\begin{aligned}
A_{xx} &= A_s - A_p + 3A_p \sin^2\theta \cos^2\phi \\
A_{yy} &= A_s - A_p + 3A_p \sin^2\theta \sin^2\phi \\
A_{zz} &= A_s - A_p + 3A_p \cos^2\theta \\
A_{xy} &= A_{yx} = 3A_p \sin^2\theta \sin\phi \cos\phi \\
A_{xz} &= A_{zx} = 3A_p \sin\theta \cos\theta \cos\phi \\
A_{yz} &= A_{zy} = 3A_p \sin\theta \cos\theta \sin\phi
\end{aligned} \tag{11}$$

Here we have chosen the frame of axes (x,y,z) in accordance with our earlier work and Fig. 1; θ is the angle between the Gd^{3+}-F^- axis and the z axis; and ϕ is the angle between the projection of the Gd^{3+}-F^- axis in the xy plane and the x axis; A_s and A_p are the isotropic and the anisotropic hfs constants, respectively (see also Bill[11] and Baker and Christidis[12]). Covalency and overlap will cause relative changes in A_s and A_p and this makes it hard to estimate the positions of the nearest F^- ions relative to the Gd^{3+} position. It has been suggested by Baker and Christidis[13] that the electrostatic polarization caused by the presence of excess charges may give rise to significant contributions to the superhyperfine interaction associated with nearest neighbors. These contributions can be represented as follows

$$\mathcal{H}_{\text{pol}} = \sum_{i,j,k} F_{ijk} E_i S_j I_k \ , \tag{12}$$

where E_i are the components of the local electric field at the defect. It can be shown that for the F^- ions of the first coordination shell there are at least eight F_{ijk} which are unequal to zero. It is easy to see that the contributions given in Eq. (12) give rise to extra terms in the expression for A_{jk} [Eq. (11)]. Arkhipov *et al.*[14] have investigated the effect of polarization induced by an externally applied electric field on the superhyperfine interaction of the nearest neighbors of Gd^{3+} in CaF_2. These authors have studied samples with applied fields as high as 50 kV/mm. The largest shifts of the ENDOR lines were 30 kHz. For the F^- ions neighboring both Gd^{3+} and Li^+ the additional electric field caused by the orthorhombic symmetry of the center is calculated to be 1.7×10^{10} V/m; extrapolating the experimental results of Arkhipov *et al.* we find additional shifts of the order of 3 MHz. For Gd^{3+}-K^+ complexes the corresponding electric field is more than a factor of 3 smaller and therefore the shifts associated with polarization are

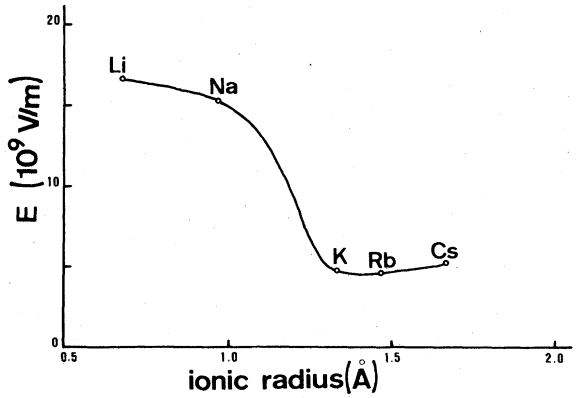

FIG. 6. Calculated additional electric field strength at ions b (see Fig. 5) relative to the field strength found for cubic Gd^{3+}, as a function of the ionic radius of the M^+ ion.

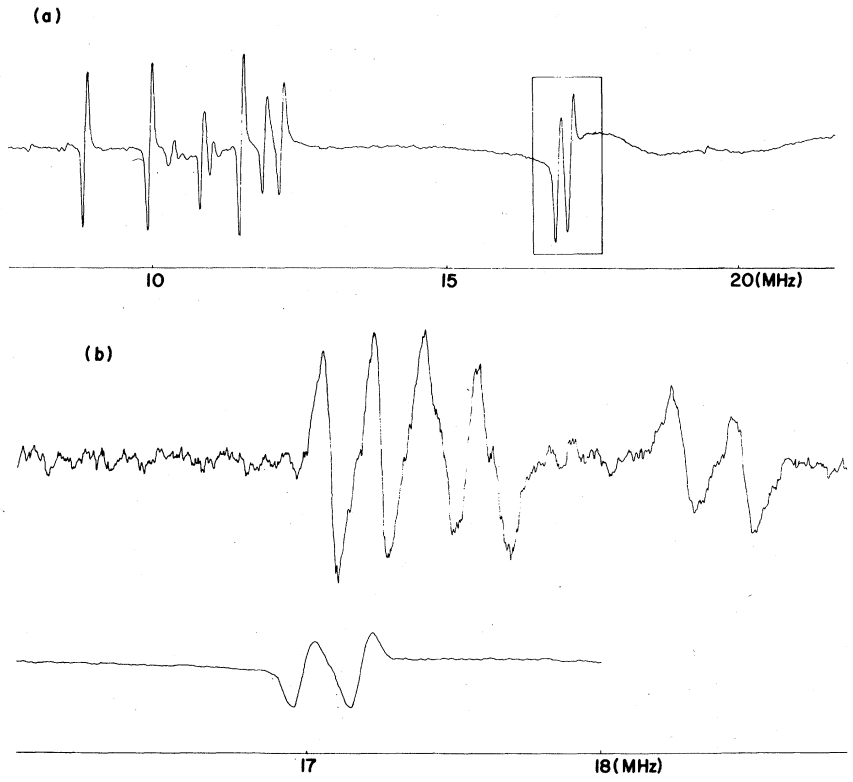

FIG. 7. (a) ENDOR spectrum obtained from the $S_z = \frac{3}{2} \leftrightarrow \frac{1}{2}$ transition of cubic Gd^{3+} in CaF_2. The magnetic field strength is 2638 G and $\vec{H} \parallel [100]$. The z axis of the complex is along [011] or [0$\bar{1}$1] (the corresponding EPR lines coincide). The rf field is along [011]. The ENDOR line indicated in this figure corresponds with nuclei in the first coordination shell. It shows a splitting due to a minor misorientation of the magnetic field. This line has been given in detail in (b). (b) The indicated ENDOR lines of (a) have been given in the lower part of the figure. In the upper part of the figure the corresponding ENDOR lines for a Gd^{3+}-Li^+ complex have been given (EPR line at 2841 G). These lines have split up into three groups corresponding with the three groups of nuclei (a, b, and c) in the first coordination shell (see Fig. 5).

smaller. In Fig. 6 we have plotted the electric field strength at the F^- ions mentioned as a function of the M^+ radius. The magnitude of the polarization effect is such that it is quite difficult to calculate the ionic positions of the first shell F^- ions from the observed hyperfine parameters A_{jk}.

For Gd^{3+}-K^+ complexes we have analyzed the shifts of the ENDOR lines associated with the ions a, b, and c (see Fig. 5). In Fig. 7 we given an example of our ENDOR results on Gd^{3+} in CaF_2:Li^+. For one of the lines we show the observed shifts due to the presence of the charge compensator. Considering these shifts for centers of orthorhombic symmetry one should realize that the crystal-field terms such as $B_2^0 O_2^0$ and $B_2^2 O_2^2$ give rise to a splitting as compared to the cubic situation. These splittings can be calculated because the crystal-field parameters are known (see Ref. 2). We have found that the elements of the superhyperfine tensors for CaF_2:Gd^{3+},K^+ can be satisfactorily described by formulas (11). The largest shifts observed are of the order of 2 MHz and typical deviations between the observed and calculated values are about 5% of the experimentally determined shifts. An analysis of the results for the first shell F^- ions of Gd^{3+}-Li^+ complexes in CaF_2 reveals that formulas (11) can no longer be maintained. This is probably due to the polarization effect, which is expected to be significantly larger for Gd^{3+}-Li^+ complexes than for Gd^{3+}-K^+ because, as mentioned above, the electric field is relatively large for Gd^{3+}-Li^+. The results of the calculation for ions b and c of A_s, A_p, and θ are given in Table V.

From Table V we see that the ions b show the largest deviations of the superhyperfine interactions as compared to the cubic situation. This agrees with the conclusions drawn from earlier experimental results where we found that the ions b relax appreciably away from the positions corresponding with cubic Gd^{3+}. The present results suggest that for Gd^{3+}-K^+ complexes the superhyperfine interaction between the

TABLE V. Superhyperfine parameters of ions b and c (see Fig. 5) for a Gd^{3+}-K^+ complex in CaF_2 including the parameters for cubic Gd^{3+}.

	Ion b	Ion c	Cubic (ion b and c)[a]
A_s (MHz)	−2.55	−1.58	−1.89
A_p (MHz)	5.28	5.00	5.08
θ (deg)	4.2	0.3	0

[a]See Ref. 12.

electron system and the nearest F nuclei is determined mainly by overlap and covalency, which can be described in terms of A_s and A_p. This situation makes a reliable calculation of the ionic positions impossible. It is clear from the above discussion that for Gd^{3+}-Li^+ complexes the situation is even worse because of the polarization effects. If one would carry out many highly accurate ENDOR experiments one would be able to determine the values A_{jk}, but it is impossible to interpret the results in a straightforward way.

The second and third shell ^{19}F nuclei show much simpler hyperfine interaction with the Gd^{3+} $4f^7$ electron configuration. The hyperfine interaction is of predominantly anisotropic nature and originates from the classical dipole-dipole interaction. The ENDOR lines observed for the F nuclei of the second and third shell shift because the Gd^{3+} ion has moved away from the substitutional site; from Fig. 5 one observes that some of these nuclei are well separated from the charge compensation center and therefore the shifts of these F^- positions from the positions corresponding with the cubic Gd^{3+} center will be small. Starting with these assumptions, the shift of the cubic Gd^{3+} ion towards the neighboring K^+ impurity becomes 0.03 Å. This conclusion could be drawn from ENDOR results of F^- ions located at 113, 131, 311 (second shell) with respect to a Gd^{3+}-K^+ complex with Gd^{3+} at 000 and K^+ at $0\bar{2}2$.

Another interesting result for the ions of the second shell of F^- ions is obtained if one considers the hyperfine interaction associated with ion d. Our results indicate that these ions have shifted over a relatively large distance (0.28 Å) outwardly with respect to the defect. From Fig. 5 we immediately see that indeed one of these ions is a nearest neighbor of the K^+ impurity. For the ions of the third coordination shell we have observed ENDOR lines that, as a result of the large Gd–F distance, have shifted only very slightly from the positions calculated for cubic Gd perturbed by an orthorhombic crystal field. From the observed line positions we have to conclude that the shift of the Gd^{3+} from the cubic position is less than 0.04 Å, which is not in contradiction with the shift obtained for the ENDOR lines associated with the second shell nuclei. This result has been obtained from the F^- ions at 133, 313, and 331 of the Gd^{3+}-K^+ center described above. In Table VI we have compiled the shifts obtained for various ions in the close neighborhood of the Gd^{3+}-K^+ complex in CaF_2.

IV. DISCUSSION

From the results it is obvious that the EFE is large for small M^+ impurities. Consequently, the contribution of the odd crystal-field terms to the even crystal field will be of interest especially for Gd^{3+}-Li^+, Gd^{3+}-Na^+, and Gd^{3+}-Ag^+ complexes in CaF_2. In ad-

TABLE VI. Shifts for some ions in the neighborhood of a Gd^{3+}-K^+ complex in CaF_2, obtained by means of ENDOR. The position of the Gd^{3+} ion is 000, the position of the K^+ ion is $0\bar{2}2$. Some ions are indicated by characters which correspond with those in Fig. 5.

	Ion	Displacement (relative to the Gd^{3+} position)
	$\bar{1}\bar{1}3$, d	0.28 Å away from the K^+ ion (radial)
	113, e	0.03 Å antiparallel to z
Second	131	0.03 Å antiparallel to z
shell	$3\bar{1}\bar{1}$	0.04 Å towards the Gd^{3+} ion (radial)
	311	< 0.05 Å
	$\bar{1}3\bar{1}$	< 0.05 Å
	133	< 0.04 Å
Third	313	< 0.04 Å
shell		
	331	< 0.04 Å

dition we note that, just for these systems, the B_2^0 values turn out to be rather small, implying that certainly for this group of defects it is necessary to take into account these contributions. It is easy to show that the introduction of the second-order term in Eq. (5) for Gd^{3+}-Li^+ complexes leads to a change of sign of B_2^0. We have accounted for this effect in a straightforward way in terms of the electrostatic model. We emphasize that in the superposition model, which is used frequently today, this effect is neglected[15]; because of this, the superposition model is inadequate to deal with the second degree crystal-field parameter B_2^0 in the case of Gd^{3+}-M^+ complexes. Similar agreement might hold for the other systems studied in the literature; thus, if the Gd^{3+} ion is located at a position without inversion symmetry, in general higher-order contributions to B_2^0 and B_2^2 associated with odd crystal-field interaction cannot be neglected. In these particular cases a more detailed investigation including the EFE is necessary.

In the present study we have investigated the consequences of variations of the coefficients occurring in Eqs. (3) and (4), which have been derived in Refs. 2 and 4. Our conclusions drawn from these studies are: (i) the proportionality factor associated with c_2^0 should be approximately correct; (ii) the proportionality factor connected with the term $(c_1^0)^2$ is too small.

Reviewing the results obtained up to now we conclude that, although there is some uncertainty about the odd field contributions, the general description of the experimental results as given by the electrostatic model is quite satisfactory. In addition, we emphasize that the F^- displacements found in accordance with the various proportionality factors follow roughly the same general trend when the M^+ radius is increased (see Tables III and IV). Compared with the results published earlier[2] the values given in this paper show slight deviations. Whereas $\Delta z(F)$ in our earlier work increased with increasing M^+ radius, it reveals a decrease with increasing M^+ radius in the present paper. We note that, as before, the variations in $\Delta z(F)$ as a function of the M^+ radius are small. Our calculations show that the iterative treatment of the polarization effect causes the discrepancy between the present results and those published in Ref. 2. The most obvious effect deduced from the crystal-field measurements and the EFE experiments is the increasing outward x shift of the fluorine ions neighboring both the Gd^{3+} and the M^+ impurity with the increasing M^+ radius.

An interesting conclusion that can be drawn from the theoretical calculations of B_2^0, B_2^2, and the ionic shifts is that the influence of dipole-dipole interaction between the induced dipoles on the crystal-field interaction is quite significant. Although here we are dealing with effective charges and dipoles in a polarizable crystal and one might expect the induced dipoles to be of importance, we feel that this also applies to systems where one has large misfits between the sizes of the impurity ions and the ions of the host material. Thus, one should be careful with the interpretation of the observed crystal-field splitting parameters whenever the valency of the magnetic impurity deviates from that of the ions of the host crystal. Moreover, the effect of displacement dipoles resulting from relaxations in the neighborhood of the defect will give rise to an interacting system of induced dipoles, which contributes to the crystal field at the central magnetic impurity.

The method employed to interpret the observed crystal-field parameters B_2^0 and B_2^2 and the EFE in terms of displacements of the central Gd^{3+} impurity and two of the neighboring fluoride ions, contains approximations. A very important deficiency of the model is that we have ignored the shifts of the other neighboring ions; because of the long-range character of the Coulomb interaction this may contribute considerably to the crystal-field parameters and the EFE. Considering a series of Gd^{3+}-M^+ complexes we are able to eliminate this inaccuracy by looking at the trends of the parameters mentioned above as a function of the M^+ radius. The variations of B_2^0, B_2^2, and the EFE are due to variations of the *short-range* repulsive interactions associated with the different M^+ impurities.

Our ligand ENDOR experiments have provided useful information about the shifts of the various lattice ions neighboring the charge compensation center. These experiments have demonstrated that for Gd^{3+}-K^+ complexes in CaF_2 the Gd^{3+} impurity has shifted about 0.03 Å towards the K^+ ion. The position of the Gd^{3+} ion was measured by comparing the ligand hyperfine interactions between the $4f^7$ electron system and distant ^{19}F nuclei for cubic orthorhombic Gd^{3+} impurities.

The interaction between the central Gd^{3+} $4f^7$ electron system and the nearest neighbor ^{19}F nuclei can be determined rather accurately with ligand ENDOR experiments, but the interpretation remains too complicated and therefore the shifts of these ions away from the "cubic positions" cannot be calculated. For more distant ions, however, ENDOR results may lead to a rather accurate calculation of the ionic positions. We have observed appreciable displacements for the ions in the second coordination shell of Gd^{3+} neighboring the K^+ impurity (see also Fig. 5; ions referred to as *d*). The shift of the central Gd^{3+} ion is in fair agreement with the results given in Table III, which were derived independently from EFE and EPR experiments. The Gd^{3+} displacement as shown in Table IV, however, is a factor of 3 larger than the ENDOR value, from which we conclude that the relation between the magnetic parameters B_2^0 and B_2^2 and the electrostatic parameters c_2^0, c_2^2, and c_1^0 are best described by Eqs. (5) and (6).

APPENDIX

In order to calculate the second degree crystal-field parameters B_2^0 and B_2^2, according to Eqs. (5) and (6), we should know the electrostatic parameters c_1^0, c_2^0, and c_2^2, which can be given by

$$c_1^0 = \frac{e}{4\pi\epsilon_0}\sum_i \frac{Q_i Z_i}{R_i^3} ,$$
$$c_2^0 = \frac{e}{16\pi\epsilon_0}\sum_i \frac{Q_i(3Z_i^2 - R_i^2)}{R_i^5} , \quad \text{(A1)}$$
$$c_2^2 = \frac{3e}{16\pi\epsilon_0}\sum_i \frac{Q_i(X_i^2 - Y_i^2)}{R_i^5} ,$$

where we have only taken into account the monopole contributions, due to the charges $Q_i e$, located at positions $\vec{R}_i$ with respect to the Gd^{3+} position. We have also considered contributions from induced dipoles, which can also be written in the form of lattice sums as given in Eq. (A1),

$$c_l^m(\text{dipoles}) = \sum_i \frac{\partial c_l^m}{\partial X_i}\frac{\alpha_i E_x^{(i)}}{eQ_i} + \sum_i \frac{\partial c_l^m}{\partial Y_i}\frac{\alpha_i E_y^{(i)}}{eQ_i} + \sum_i \frac{\partial c_l^m}{\partial Z_i}\frac{\alpha_i E_z^{(i)}}{eQ_i} . \quad \text{(A2)}$$

Here, α_i is the polarizability of ion i and $E_x^{(i)}$, $E_y^{(i)}$, and $E_z^{(i)}$ are the components of the electric field at ion i. In order to calculate c_l^m(dipoles) it is necessary to evaluate the electric fields $\vec{E}^{(i)}$. The electric field consists of two important contributions: (i) the contributions due to the monopoles ($\vec{E}_m^{(i)}$); (ii) the contributions due to the induced dipoles ($\vec{E}_d^{(i)}$). The electric field contributions can be given in the form of lattice sums

$$\vec{E}_m^{(i)} = \frac{e}{4\pi\epsilon_0}\sum_{j\neq 1}\frac{Q_i(\vec{R}_i - \vec{R}_j)}{|\vec{R}_i - \vec{R}_j|^3} , \quad \text{(A3)}$$

$$\vec{E}_d^{(i)} = -\frac{1}{4\pi\epsilon_0}\sum_{j\neq i}\left(\frac{\alpha_j(\vec{E}_m^{(j)} + \vec{E}_d^{(j)})}{|\vec{R}_i - \vec{R}_j|^3} - 3\frac{\alpha_j(\vec{R}_i - \vec{R}_j)\cdot(\vec{E}_m^{(j)} + \vec{E}_d^{(j)})}{|\vec{R}_i - \vec{R}_j|^5}\cdot(\vec{R}_i - \vec{R}_j)\right) . \quad \text{(A4)}$$

Formula (A4) shows that in order to evaluate the electric field at an ion j one should know the electric field strengths at all other ions in the lattice. In order to limit the computing times it is useful to divide the crystal into three regions I, II, and III. In region I, in the close vicinity of the dipolar defect, the positions and charges of the ions deviate from those corresponding with the perfectly cubic situation. In region II the ions are located at the perfect lattice positions; in regions I and II the induced dipoles influence each other. As we have three independent EPR parameters to fit, we must confine ourselves to systems in which region I contains four ions, i.e., the Gd^{3+} impurity, the two lattice fluoride ions neighboring both Gd^{3+} and M^+ (ion b), and M^+ impurity; region II contains about 400 ions. Region III contains 2000 ions of which the induced dipole moments do not interact with each other.

It is easy to see that Eq. (A3) can be written as follows:

$$\vec{E}_m^{(i)} = \frac{e}{4\pi\epsilon_0}\left(\sum_{\substack{j\in \mathrm{I}\\ j\neq i}}\frac{Q_j(\vec{R}_i - \vec{R}_j)}{|\vec{R}_i - \vec{R}_j|^3} - \sum_{\substack{j\in \mathrm{I}\\ j\neq i}}\frac{Q_j^c(\vec{R}_i - \vec{R}_j^c)}{|\vec{R}_i - \vec{R}_j^c|^3}\right) + \vec{E}_{\text{lattice}}(\vec{R}_i - \vec{R}_i^c) , \quad \text{(A5)}$$

In the first term we take into account the fact that the ions in region I relax towards new positions; also, the deviating charges of the impurities Gd^{3+} and M^+ are accounted for; Q_j is the actual valency of the ions in region I, whereas Q_j^c are the valencies of the corresponding ions in the perfect lattice. A Taylor-series expansion of the electrostatic potential of the unperturbed lattice has been given by van Winsum *et al.*[16] From these potentials we can calculate the electric field as a function of the displacement of the ions in region I. This contribution is given by the last term in Eq. (A5); if i is chosen such that the ion is located in region II, $\vec{E}_{\text{lattice}}(\vec{R}_i) = 0$.

The contributions $\vec{E}_d^{(i)}$ are calculated using Eq. (A4) with first $\vec{E}_d^{(j)} = 0$. If $\vec{E}_d^{(i)}$ is calculated for all values of i ($i = 1-400$), these values are substituted in Eq. (A4) to evaluate a new set of $\vec{E}_d^{(i)}$'s. These values are employed to find a new set of $\vec{E}_d^{(i)}$'s, etc. This procedure leads to self-consistent electric field strengths, which may be used to calculate the dipolar contributions to the electrostatic parameters c_l^m by substituting the total electric field strength into Eq. (A2).

We have found that in general the convergence of the lattice sums as given in Eq. (A1) can be improved by calculating the deviation between the electrostatic contributions corresponding with cubic Gd^{3+} and orthorhombic Gd^{3+}-M^+ centers. As an example we give the expression for c_1^0:

$$c_1^0 = \frac{e}{4\pi\epsilon_0}\sum_i\left(\frac{Q_i Z_i}{R_i^3} - \frac{Q_i^c Z_i^c}{(R_i^c)^3}\right) . \quad \text{(A6)}$$

From the symmetry arguments it is easy to show that the sum over the lattice term in Eq. (A6) is zero.

It should be emphasized that the polarization effects discussed above give quite large contributions to the crystal-field parameters c_1^0, B_2^0, and B_2^2. A review

TABLE VII. Crystal-field parameters as calculated using some different electrostatic methods.

	c_1^0 (10^9 V/m)	B_2^0 (G)	B_2^2 (G)
1. Point charge of M^+ only	−9.7	−81.5	0
2. Point charges of Gd^{3+} and M^+ and 2000 induced dipoles (noninteracting)	−4.1	−40.4	−141.3
3. Same as 2; region II contains 50 interacting dipoles	−5.7	−41.5	−98.8
4. Same as 2; region II contains 100 dipoles	−5.9	−43.1	−91.6
5. Same as 2; region II contains 400 dipoles	−6.2	−42.8	−89.6

of some simple results of our calculations has been given in Table VII. During these calculations we have observed that accurate values of the electric field strengths are obtained of 400 interacting dipoles after three iterations. The results shown in Table VII have been obtained for a rigid lattice; it should be noted, that similar observations have been made for situations in which the lattice surrounding the defect is allowed to relax.

ACKNOWLEDGMENTS

The authors wish to thank P. Wesseling for growing the crystals used in this investigation. This work is part of the research program of the Stichting voor Fundamenteel Onderzoek der Materie and has been made possible by financial support from the Nederlandse Organisatie voor Zuiver Wetenschappelijk Onderzoek.

[1]E. J. Bijvank and H. W. den Hartog, Phys. Rev. B 12, 4646 (1975).
[2]E. J. Bijvank, H. W. den Hartog, and J. Andriessen, Phys. Rev. B 16, 1008 (1977).
[3]A. N. Lefferts, E. J. Bijvank, and H. W. den Hartog, Phys. Rev. B 17, 4214 (1978).
[4]E. J. Bijvank, A. G. Zandbergen-Beishuizen, and H. W. den Hartog, Solid State Commun. 32, 239 (1979).
[5]W. B. Mims, *The Linear Electric Field Effect in Paramagnetic Resonance* (Clarendon, Oxford, 1976).
[6]R. Parrot, Phys. Rev. B 9, 4660 (1974).
[7]A. Kiel, Phys. Rev. 148, 247 (1966).
[8]A. Kiel and W. B. Mims, Phys. Rev. 153, 378 (1967).
[9]C. A. Hutchison, B. R. Judd, and D. F. D. Pope, Proc. Phys. Soc. London Sect. B 70, 514 (1957).
[10]B. G. Wybourne, Phys. Rev. 148, 317 (1966).
[11]H. Bill, Phys. Lett. 29A, 593 (1969).
[12]J. M. Baker and T. Christidis, J. Phys. C 10, 1059 (1977).
[13]J. M. Baker and T. Christidis, Phys. Lett. 59A, 171 (1977).
[14]S. M. Arkhipov, N. V. Legkikh, B. Z. Malkin, and Yu. A. Sherstkov, Sov. Phys. JETP 47, 896 (1979).
[15]D. J. Newman and W. Urban, Adv. Phys. 24, 793 (1975).
[16]J. A. van Winsum, H. W. den Hartog, and T. Lee, Phys. Rev. B 18, 178 (1978).